Amino Acids (2011) 40:765–779
DOI 10.1007/s00726-010-0645-9

ORIGINAL ARTICLE

Human Alzheimer's disease synaptic *O*-GlcNAc site mapping and iTRAQ expression proteomics with ion trap mass spectrometry

Yuliya V. Skorobogatko · John Deuso · Jared Adolf-Bergfoyle · Matthew G. Nowak · Yuesong Gong · Carol Frances Lippa · Keith Vosseller

Received: 28 April 2010 / Accepted: 27 May 2010 / Published online: 19 June 2010

Abstract Neuronal synaptic functional deficits are linked to impaired learning and memory in Alzheimer's disease (AD). We recently demonstrated that *O*-GlcNAc, a novel cytosolic and nuclear carbohydrate post-translational modification, is enriched at neuronal synapses and positively regulates synaptic plasticity linked to learning and memory in mice. Reduced levels of *O*-GlcNAc have been observed in AD, suggesting a possible link to deficits in synaptic plasticity. Using lectin enrichment and mass spectrometry, we mapped several human cortical synaptic *O*-GlcNAc modification sites. Overlap in patterns of *O*-GlcNAcation between mouse and human appears to be high, as previously mapped mouse synaptic *O*-GlcNAc sites in Bassoon, Piccolo, and tubulin polymerization promoting protein p25 were identified in human. Novel *O*-GlcNAc modification sites were identified on Mek2 and RPN13/ADRM1. Mek2 is a signaling component of the Erk 1/2 pathway involved in synaptic plasticity. RPN13 is a component of the proteasomal degradation pathway. The potential interplay of phosphorylation with mapped *O*-GlcNAc sites, and possible implication of those sites in synaptic plasticity in normal versus AD states is discussed. iTRAQ is a powerful differential isotopic quantitative approach in proteomics. Pulsed Q dissociation (PQD) is a recently introduced fragmentation strategy that enables detection of low mass iTRAQ reporter ions in ion trap mass spectrometry. We optimized LTQ ion trap settings for PQD-based iTRAQ quantitation and demonstrated its utility in *O*-GlcNAc site mapping. Using iTRAQ, abnormal synaptic expression levels of several proteins previously implicated in AD pathology were observed in addition to novel changes in synaptic specific protein expression including Synapsin II.

Keywords *O*-GlcNAc · Alzheimer's disease · Proteomics · iTraq · Post-synaptic density

Introduction

Alzheimer's disease (AD) accounts for about 50% of dementias and involves progressive loss of the ability to form and store memories. It is now clear that early synaptic dysfunction occurs in AD prior even to the formation of hallmark Aβ plaque and neurofibrillary tangle (NFT) pathology (LaFerla and Oddo 2005; Selkoe 2002). Soluble forms of Aβ prior to plaque deposition have been linked to synaptic deficits such as reduced long-term potentiation (LTP), an electrophysiological read-outs of synaptic plasticity thought to correlate with some forms of learning/memory (Gylys et al. 2004; Rowan et al. 2003; Lacor et al. 2004; Oddo et al. 2003), but the molecular basis for these synaptic deficits are not clear.

O-GlcNAc is a single *N*-acetylglucsosamine carbohydrate *O*-linked to serines and threonines of cytosolic and nuclear proteins. Analogous to the way kinases and phosphatases regulate phosphorylation, cytosolic and nuclear enzymes dynamically catalyze addition (OGT) and

Electronic supplementary material The online version of this article (doi:10.1007/s00726-010-0645-9) contains supplementary material, which is available to authorized users.

Y. V. Skorobogatko · J. Deuso · J. Adolf-Bergfoyle · M. G. Nowak · K. Vosseller (✉)
Department of Biochemistry and Molecular Biology, Drexel University College of Medicine, Philadelphia, USA
e-mail: Keith.Vosseller@DrexelMed.edu

Y. Gong · C. F. Lippa
Department of Neurology, Drexel University College of Medicine, Philadelphia, USA

removal (*O*-GlcNAcase) of *O*-GlcNAc (Gao et al. 2001; Kreppel et al. 1997).

O-GlcNAc levels are especially high at neuronal synapses (Akimoto et al. 2003; Cole and Hart 2001; Tallent et al. 2009). In mice, site-specific *O*-GlcNAc modification was observed on proteins that regulate availability of synaptic vesicles for release (e.g. Bassoon and Piccolo), and on other signaling molecules known to play a role in synaptic plasticity (e.g. Synaptic Ras-GTPase) (Vosseller et al. 2006). In vivo elevation of *O*-GlcNAcation in mice enhances hippocampal LTP/synaptic plasticity (Tallent et al. 2009). Thus, *O*-GlcNAc may be a novel positive regulator of synaptic signaling underlying learning and memory.

Reduced *O*-GlcNAcation has been implicated in AD. *O*-GlcNAc levels are reduced in post-mortem human AD brain (Liu et al. 2004) and on specific synaptic proteins such as AP180 (Yao and Coleman 1998) and CRMP-2 (Kanninen et al. 2004). Reduced *O*-GlcNAcation in human AD may be related to metabolic changes in AD. *O*-GlcNAc is a known "nutritional" sensor, as levels of *O*-GlcNAcation respond to glucose availability through hexosamine biosynthetic pathway (HBP) flux (Wells et al. 2003). Glucose metabolism/uptake is reduced in AD (Schubert 2005) and thus reduced flux through the HBP in AD may contribute to reduced *O*-GlcNAcation. Reduced *O*-GlcNAcation has been implicated in the AD pathology of NFT formation. AD related hyperphosphorylation of Tau leads to its aggregation in NFTs. Tau is modified by *O*-GlcNAc (Arnold et al. 1996), and decreased *O*-GlcNAc in AD is associated with reciprocal Tau hyperphosphorylation. Elevation of *O*-GlcNAcation reduces specific Tau hyperphosphorylation events in vivo (Li et al. 2006; Liu et al. 2004, 2009; Yuzwa et al. 2008). Thus, a specific link between reduced *O*-GlcNAc and NFT pathology is indicated. Given the enrichment of *O*-GlcNAc at neuronal synapses, and its role in synaptic plasticity, it is possible that abnormal *O*-GlcNAcation may contribute to human AD synaptic deficits underlying learning and memory defects.

iTRAQ is a differential isotopic labeling approach in quantitative comparative proteomics (Ross et al. 2004; Ong and Mann 2005). Amine reactive iTRAQ tags are isobaric, but give rise to differential isotopic quantitative reporter ions in MS/MS. iTRAQ is suited for post-translational modification analysis as all peptides are labeled at the N-terminus. iTRAQ depends on detection of reporter ions at relatively low *m*/*z* (e.g. 114–117) in MS/MS scans, which traditionally is problematic in ion trap mass spectrometry due to the so-called "1/3" rule in which ions of $m/z < 1/3$ of the precursor *m*/*z* are usually not detected (Cunningham et al. 2006). A recently introduced fragmentation strategy called pulsed Q dissociation (PQD) allows for detection of low mass iTRAQ reporter ions in ion trap mass spectrometry (Schwartz et al. 2005). PQD has been utilized in quantitative proteomics using iTRAQ in an ion trap mass spectrometry (Griffin et al. 2007; Meany et al. 2007; Bantscheff et al. 2008; Guo et al. 2008), but the effectiveness of PQD in peptide sequencing is low compared to CID, and reproducibility of quantitative accuracy is highly dependent on variables such as collision energy.

Here, we targeted a human cortical synaptic fraction for *O*-GlcNAc site mapping and AD expression proteomics. *O*-GlcNAc sites mapped suggest potential interplay with regulatory phosphorylation in signaling linked to synaptic vesicle dynamics and synaptic plasticity. Additionally, we validated compatibility of iTRAQ with ion trap mass spectrometry and *O*-GlcNAc site mapping, and identified an altered expression pattern in a human AD cortical synaptic sample.

Materials and methods

Post-synaptic density fractionation

Synaptosomes and post-synaptic densities (PSD) were isolated from human AD and control frontal cortical tissues as described (Carlin et al. 1980; Gong et al. 2009). Briefly, tissues were homogenized in buffer A (0.32 M sucrose–5 mM HEPES, pH 7.4, 1 mM $MgCl_2$, 0.5 mM $CaCl_2$ and protease inhibitors) with a Teflon homogenizer. The resultant homogenates were centrifuged at 1,400*g* × 10 min. The pellets were re-homogenized in the same buffer A and centrifuged at 700*g* × 10 min. The combined supernatants were centrifuged at 13,800*g* × 10 min. The pellets were resuspended in 6 mM Tris–HCl buffer with 0.32 M sucrose and protease inhibitors, pH 8.0, loaded onto sucrose gradient (0.85/1/1.15 M in 6 mM Tris–HCl, pH 8.0) and centrifuged at 82,500*g* × 120 min. The synaptosomes were collected from the interface between 1 and 1.15 M for analysis and PSD preparation.

Proteolytic digestion of PSD and alpha and beta casein samples, and iTRAQ labeling

PSD lysates (100 μg) or a mixture of alpha and beta casein (resuspended in 6 M urea buffer) was digested in 50 mM ammonium bicarbonate buffer, pH 8.0 using sequence-grade modified trypsin (Promega, Madison, WI) following reduction by 10 mM dithiothreitol (Sigma-Aldrich) for 1 h at 57C°and alkylation by 50 mM iodoacetamide (Sigma-Aldrich) for 1 h at room temperature in the dark. Twenty-five micrograms aliquots of digested samples were dried in centrifugal vacuum concentrator. The synthetic *O*-GlcNAc modified peptide PSVPV(*S*-*O*-GlcNAc)GSAPGR was a

kind gift of Dr. Gerald Hart, Johns Hopkins School of Medicine. The procedure for iTRAQ labeling was as according to the manufacturer's protocol (Applied Biosystems Inc.). Two reactions were set up: one with 114 and one with 117 labels. Briefly, a quarter of an iTRAQ label vial (114 or 117) was used to label 25 μg of protein in total reaction volume of 25 μl (approximately 2.5 μl of iTRAQ label, 70% ethanol, 25 μg of protein dissolved in iTRAQ dissolution buffer). Samples were incubated for 1 h at room temperature, mixed and dried down.

HPLC fractionation

iTRAQ labeled PSD samples were injected into a Akta Purifier (GE Healthcare) and loaded onto a TriCon MonoS 5/50 G1 strong cation exchange (SCX) column (GE Healthcare). Sample was washed with buffer A (5 mM KH_2PO_4, 30% acetonitrile, pH 2.7) and then eluted with a 40-min gradient of buffer B (5 mM KH_2PO_4, 30% acetonitrile, 350 mM KCl, pH 2.7). Eight different peptide containing fractions were collected. The sample volumes were reduced twice on centrifugal vacuum concentrator to evaporate acetonitrile and then were desalted using C18 Zip-Tips (Millipore, Billerica, MA), dried, and re-suspended in LC–MS loading buffer (0.1% formic acid). In the case of iTRAQ labeled alpha and beta casein mix, the sample was directly desalted over C18 Zip-Tips.

Lectin weak affinity chromatography enrichment of *O*-GlcNAc peptides

Wheat germ agglutinin (WGA)-based enrichment of *O*-GlcNAc modified peptides was performed as described (Vosseller et al. 2006). Briefly, WGA coupled to agarose (Vector Laboratories) washed with WGA buffer (25 mM Tris, pH 7.8, 300 mM Nacl, 5 mM $CaCl_2$, 1 mM $MgCl_2$) was packed into an opaque 20 m length of Teflon tubing with O.D. 1.59 mm and I.D. 0.1 mm (Upchurch Scientific) which was fitted with Peek unions at its ends containing 0.5 μm frits to create a column. Five hundred micrograms of human PSD digested with trypsin, was desalted with macrospin C18 columns (Nest), suspended in 40 μl of WGA buffer, and loaded on an AKTA Purifier (Amersham) HPLC. *O*-GlcNAc modified peptides were enriched by an isocratic 100% WGA buffer at a flow rate of 0.15 ml/min, monitored by UV absorbance at 214, 256, and 280, and 1 min fractions were collected. Combined fractions of interest eluting subsequent to the major peak of non-enriched peptide were acidified by addition of 0.5% volume of formic acid and desalted using C18 Zip-Tips for subsequent LC–MS/MS analysis. During WGA isocratic chromatography, the pressure of the HPLC system has been observed to rise slowly due to the compression of agarose resin. The pressure was never allowed to exceed 5 MPa.

Nanospray ESI–LC–MS/MS analysis by linear ion trap PQD/CID

All on-line LC–MS/MS runs were completed using an Eksigent NanoLC-AS1 auto-sampler (Eksigent, Dublin, CA) inline with a LTQ linear ion trap mass spectrometer (Thermo Scientific, San Jose, CA). Samples were injected onto an IntergraFrit Proteopep II (New Objective, Woburn, MA) C18 sample trap column (300 Å × 75 μm ID × 2.5 cm bed length) for final desalting and concentration at a flow rate of 3 μl/min (0.1% formic acid) for 15 min. The inline capillary column for 2D separations was a IntegraFrit Proteopep II (New Objective, Woburn, MA) C18 column (300 Å × 75 μm ID × 10 cm bed length). Sample was eluted from the trap column by a 55 min 5–35% linear gradient of buffer B (100% acetonitrile, 0.1% formic acid), followed by a 25 min 35–80% linear gradient of buffer B to a 5 min isocratic elution at 80% buffer B at a flow rate of 300 nl/min. Collision energies, choice of fragmentation strategy [PQD or collision-induced dissociation (CID)], and data acquisition in profile versus centroid, were varied as described in results section. Dynamic exclusion was set such that if an ion was detected it was excluded from analysis for 30 s. The electrospray voltage was 1.5 kV. The mass range for MS scans was 400–2,000 Da. Data was acquired using a single microscan and a maximum inject time of 200 ms for MS, MS^2, and MS^3 scan types. MS^3 on MS/MS was specified for precursor ions showing diagnostic neutral loss of *O*-GlcNAc mass of either 102 (doubly charged precursor) or 68 (triply charged precursor).

Sequence data analysis and iTRAQ quantitation

Searches to identify peptides and proteins were performed using Sequest (Yates et al. 1995) in Bioworks (Thermo Finnigan) software. For experiments using casein alpha/beta, a sub-database of this protein was constructed and searched. For identification of human proteins in synaptic fractions, the data was searched against the human non-redundant National Center for Biotechnology Information database (NCBInr.). For peptide identification a cross-correlation (X-cor) score of 2.5 or 3.0 for doubly and triply charged precursors was required. For protein identification, two independent peptide identifications were required, except in a few cases where the X-cor score was above 3.5 for a doubly charged precursor and manual inspection of MS/MS revealed correct b and y ion series for prominent ions. The data was searched against a reverse database to

estimate false positive identification of proteins (about 1%). Searches allowed for oxidized methionine. All *O*-GlcNAc peptides were sequenced manually for the presence of y and b ion series of both unmodified and *O*-GlcNAc modified fragments in MS/MS, combined with fragment ion information in MS/MS/MS. The mass shift of iTRAQ tags (+144.0) at N-termini and on lysines was included as a constant modification, as labeling appeared to go to 100% of a sample. 1 missed tryptic cleavage was allowed. The intensities of iTRAQ ions from PQD scans were extracted using iTRACKER software (Shadforth et al. 2005) allowing for ±0.25 Da surrounding the target iTRAQ reporter ion. For a given protein identification, the average and standard deviation of all individual iTRAQ ratios of 117 (AD sample) to 114 (control) were calculated for all linked PQD scans. Instances of apparent outlier ratios were obvious in some cases. This led us to calculate a "corrected" average and standard deviation in which iTRAQ ratios equal to or greater than two standard deviations were eliminated, and the "corrected" average and standard deviation were then recalculated. A >30% change from a 1:1 iTRAQ ratio for a given protein between control and AD was required to consider it an expression level change.

Results

O-GlcNAc site-specific modification of human synaptic cortical proteins

Lysates of synaptic fractions prepared from human cortex were digested with trypsin and *O*-GlcNAc modified peptides were enriched using lectin affinity chromatography (Vosseller et al. 2006). This enriched fraction was analyzed by reverse phase micro-capillary liquid chromatography coupled to ion trap mass spectrometry (LC–MS/MS). *O*-GlcNAc is labile in CID and this results in MS/MS spectra displaying a prominent ion corresponding to the loss of the mass of *O*-GlcNAc (neutral loss) from the precursor intact peptide. Thus, data dependent settings specified MS/MS/MS (MS^3) fragmentation of ions displaying the characteristic neutral loss of *O*-GlcNAc in MS/MS (MS^2) in order to fragment the unmodified peptide backbone and increase fragment ion information for peptide sequencing (Vosseller et al. 2006).

A novel *O*-GlcNAc site was identified on RPN13 (also known as ADRM1/ARM1), a relatively newly described component of the proteasomal degradation pathway, within the peptide SQSAAVTPSSTTSSTR corresponding to

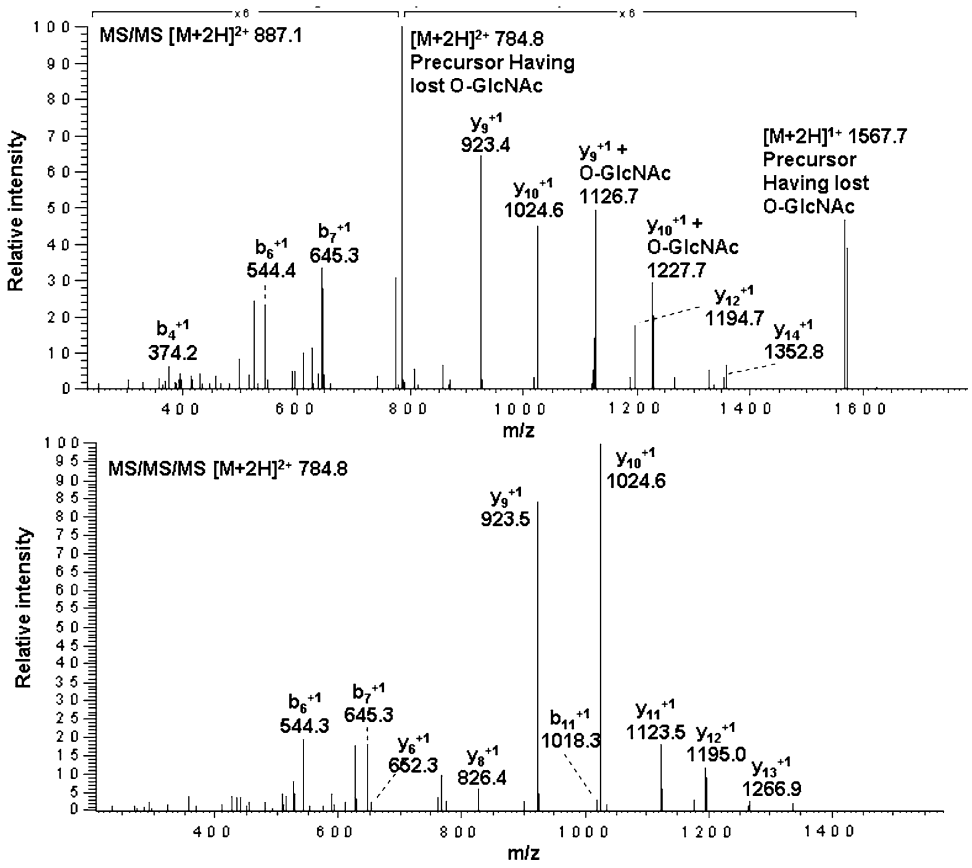

Fig. 1 Human RPN13 is *O*-GlcNAc modified within the region SQSAAVTP*SSTTSST*R at one of the residues in *italics*. Lectin enriched *O*-GlcNAc peptides from a human cortical synaptic fraction were analyzed by ion trap LC–MS/MS. The neutral loss of *O*-GlcNAc in MS/MS giving rise to the $[M+2H]^{2+}$ 784.8 and the presence of two fragment ions retaining *O*-GlcNAc modification (y9 and y10) is diagnostic of an *O*-GlcNAc modified peptide. Selection of the 784.8 *O*-GlcNAc neutral loss ion for MS/MS/MS leads to the identification of the SQSAAVTPSSTTSSTR from human RPN13

residues 211–226 (Fig. 1). The y9 fragment ion retaining *O*-GlcNAc in MS/MS indicates that the modification site is on one of seven serines/threonines in the C-terminus of the peptide from residues 219–225. This region occurs within a recognizably conserved motif for *O*-GlcNAcation (so-called PVST motif) involving a Proline and Valine proximal to multiple hydroxyl-containing amino acids. Although first described as an extracellular adhesion receptor, it is now clear that RPN13 is intracellular and functions in both recruiting the deubiquitinating enzyme UCH37 to the proteasome (Yao et al. 2006) and in acting itself as a ubiquitin receptor (Husnjak et al. 2008). Abnormal protein accumulation and aggregation may in part be due to dysfunction of the proteasome degradation system in AD (Oddo 2008). Ubiquitin is seen to accumulate in both Aβ plaques and NFTs (Ii et al. 1997) and proteasome activity is reduced in AD specifically in brain regions most affected by the disease (Keller et al. 2000). We searched the RPN13 sequence comprising the *O*-GlcNAc modified region against the "phosphosite" database (Hornbeck et al. 2004) to look for potential overlap with known phosphorylation sites in RPN13 or proteins with homology to that region. Sequence comprising the *O*-GlcNAc modified region is highly conserved between mouse, rat, and human RPN13 and is extensively phosphorylated (Table 1; Dephoure et al. 2008), indicating potential functional interplay/reciprocity between phosphorylation and *O*-GlcNAcation in this region. However, the functional significance of phosphorylation in this region is not known. Additionally, a highly conserved sequence containing the RPN13 *O*-GlcNAc modification motif was observed in the protein ASPM, a regulator of spindle assembly that when mutated leads to microcephaly (Cox et al. 2006). This region in ASPM also contains a phosphorylation site that overlaps with the motif that is homologous to the *O*-GlcNAc modified region in RPN13 (Table 1), indicating the potential interplay of *O*-GlcNAc with phosphorylation in this region. Core 26S proteasomal components have been reported to be *O*-GlcNAc modified (Sumegi et al. 2003; Klement et al. 2010) and *O*-GlcNAc is implicated in regulating proteasomal activity (Zhang et al. 2003). Possibly, altered *O*-GlcNAc modification of RPN13 might contribute to regulation of proteasomal activity in normal versus disease states such as AD.

A novel *O*-GlcNAc modification site in human MEK2 at serine 396 was identified (Fig. 2.). This site occurs on a C-terminal tryptic peptide LNQPGTPTRTAV within residues 389–400. A y6 fragment ion retaining *O*-GlcNAc in MS/MS indicates the modification occurs at either threonine 396 or 398 (Fig. 2). Fragmentation N-terminal of proline is often favored, and the abundant fragment ions in MS/MS corresponding to y6 and y9 ions both unmodified and retaining *O*-GlcNAc is consistent with this (Fig. 2). The *O*-GlcNAc neutral loss ion $[M+2H]^{2+}$ in MS/MS was selected for CID MS/MS/MS giving rise to a spectra that when combined with information from MS/MS identifies the peptide LNQPGTP***T***R***T***AV from human Mek2. The missed tryptic cleavage at the arginine in this peptide is likely due to steric hindrance by *O*-GlcNAc modification of one of the surrounding threonines, as has been previously observed (Vosseller et al. 2006). MEK is a kinase which phosphorylates Erk 1/2 (MAPK 1/2), leading to its activation. In terminally differentiated neurons, Erk is a central regulator of synaptic plasticity and learning/memory through complex influences including increased AMPA receptor insertion in membranes, regulation of ion channels, and gene expression (Sweatt 2004). The MEK2 *O*-GlcNAc site at 396/398 is proximal to a known negative regulatory phosphorylation site at 394 (Brunet et al. 1994; Xu et al. 1999; Sharma 2002). Phosphorylation of MEK2 at threonine 394 by Erk 1/2 is a negative feedback loop that downregulates MEK activity and inhibits this pathway (Brunet et al. 1994; Xu et al. 1999; Sharma 2002). Given the potential for reciprocity between *O*-GlcNAc and phosphorylation at proximal residues (Comer and Hart 2001), *O*-GlcNAc at threonine 396/398 may compete with phosphorylation of threonine 394. Potentially, decreased *O*-GlcNAcation (as may occur in Alzheimer's) may lead to "hyperphosphorylation" at the MEK negative regulatory site and thus contribute to downregulation of this pathway. Consistent with this model, we have observed that enhancement of hippocampal LTP by elevation of

Table 1 The *O*-GlcNAc modified region in RPN13 is highly conserved and overlaps with known phosphorylation sites

Protein	Accesion	Sequence homology with known phosphorylation and *O*-GlcNAcation
RPN13/ADRM1 (human)	Q16186	SSSSSRpSQpSAAVpTP**SpSpTpTSST**RATPAPSAPAAA
RPN13/ADRM1 (mouse)	Q9JKV1	SSSSSRpSQpSAAVpTP**SpSpSpTSS**ARATPAPSAPAAA
RPN13/ADRM1 (rat)	Q9JMB5	SSSSSRpSQpSAAVpTP**SpSpTpTSS**ARATPAPSAPAAA
ASPM (human)	Q8IZT6	SKSYKNEVpTP**SSTTAS**VARKRKSDG

The sequence comprising the RPN13 *O*-GlcNAcation region was searched against the phosphosite database. Known phosphorylated residues are preceded by a lower case "p". The *O*-GlcNAc modified region is in bold larger font. A region of homology was found in human ASPM with a known proximal phosphorylation site

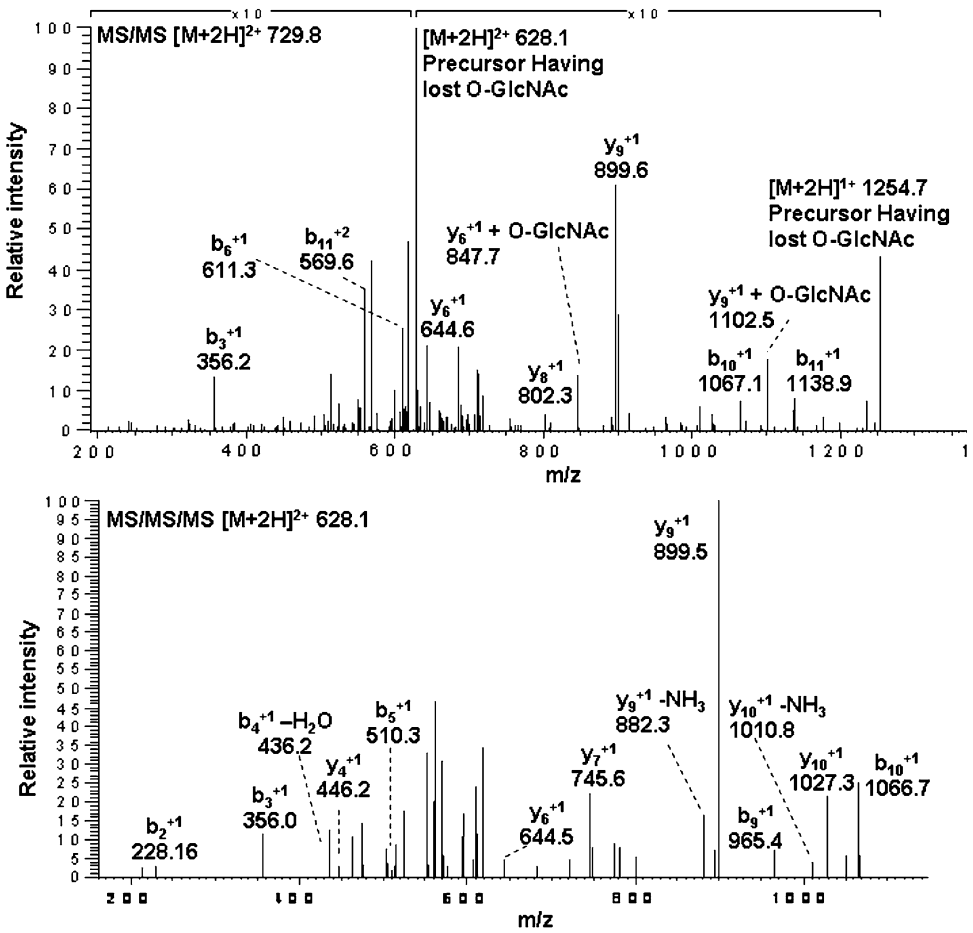

Fig. 2 Human MEK2 is *O*-GlcNAc modified at either threonine 396 or 398 within the C-terminal tryptic peptide LNQPGTP***T***R***T***AV (possible modified sites in *bold italics*). Lectin enriched *O*-GlcNAc peptides from a human cortical synaptic fraction were analyzed by ion trap LC–MS/MS. The neutral loss of *O*-GlcNAc in MS/MS giving rise to the $[M+2H]^{2+}$ 729.8 and the presence of two fragment ions retaining *O*-GlcNAc modification (y6 and y9) is diagnostic of an *O*-GlcNAc modified peptide. Selection of the $[M+2H]^{2+}$ 628.1 *O*-GlcNAc neutral loss ion for MS/MS/MS leads to the identification of the LNQPGTPTRTAV peptide from human MEK2

O-GlcNAcation is associated with increased Erk 1/2 activation (Tallent et al. 2009). Additionally, increased *O*-GlcNAcation in non-neuronal cells has been previously linked with upregulation of Erk through activation of MEK (Kneass and Marchase 2005). Potentially, interplay between MEK threonine 396/398 *O*-GlcNAcation and 394 phosphorylation may contribute to modulation of Erk activity. The amino acid sequence surrounding and including MEK threonine 394 and 396 is conserved from chicken to human, indicating potential for conserved mechanism of interplay between phosphorylation and *O*-GlcNAcation in this region (Fig. 3).

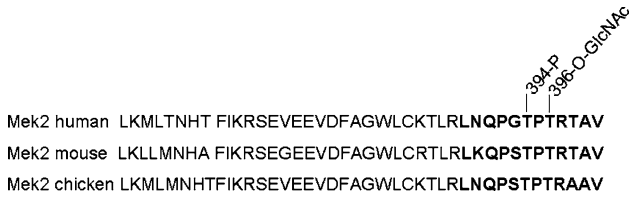

Fig. 3 Sequence alignment of *O*-GlcNAc modified region of Mek2 across species. The human Mek2 *O*-GlcNAc modified region is conserved across species, including phosphorylation site 394 and *O*-GlcNAcation site 396 (or 398, which is conserved in mouse and human, but not chicken)

An *O*-GlcNAc modification site was identified in the brain specific protein tubulin polymerization promoting protein p25 (TPPP/p25) at either serine 152 or threonine 155 within the peptide APIISGVTK (supplemental figure 1). The serine 152 site was previously identified in our proteomic screen for *O*-GlcNAc modification sites in a mouse synaptic biochemical fraction (Vosseller et al. 2006). Phosphorylation of TPPP/p25 regulates its tubulin polymerization promoting activity. TPPP/p25 is phosphorylated at serine 159 and serine 160, proximal to the *O*-GlcNAc modification site (Hlavanda et al. 2007), raising the idea of potential interplay between *O*-GlcNAc and phosphorylation on TPPP/p25 as a possible mechanism regulating its activity. TPPP/p25 has been reported to be a component of abnormal protein aggregations/inclusions in neurodegenerative disorders including Parkinson's disease and Lewy body dementias (Lindersson et al. 2005; Kovacs et al. 2007) and its abnormal expression has been linked to formation of pathological aggregates (Ovadi and Orosz 2009). Although highly speculative, potentially reduced *O*-GlcNAcation in Alzheimer's may contribute to hyperphosphorylation of proteins other than Tau (such as TPPP/

p25) and this may represent a more widespread and common influence on abnormal protein aggregation beyond Tau inclusion in NFTs.

In previous *O*-GlcNAc site mapping studies of mouse brain synapse, the proteins Bassoon and Piccolo displayed the most extensive *O*-GlcNAc modification (Vosseller 2006; Chalkley et al. 2009). Here, although a relatively small number of total human *O*-GlcNAc sites was identified, Bassoon and Piccolo *O*-GlcNAc modification was observed. Human Bassoon was observed to be *O*-GlcNAc modified at one of three threonines (residues 2,313–2,316) within the peptide EEPLP***TTT***PAAIK (supplemental figure 2). This is consistent with previously observed *O*-GlcNAc modification in the homologous region in mouse Bassoon (EEPF***STT***APAVIK). Indeed, in the mouse studies, this was one of two peptides found in a doubly *O*-GlcNAc modified state, suggesting conserved high stoichiometry *O*-GlcNAc modification in this region. A second *O*-GlcNAc site was identified on human Bassoon within the peptide GLTGPT(*T*-*O*-GlcNAc)VPATK (residues 2,925–2,938) (supplemental figure 3), consistent with previously identified *O*-GlcNAc modification of this region (GLAGPTTVPATK) in mouse Bassoon. These *O*-GlcNAcation sites are within a central domain of Bassoon (amino acids 1,692–3,263) which mediates direct interaction with the proteins CtBP1 and CAST/ELKS2 (Jose et al. 2008; Takao-Rikitsu et al. 2004; tom Dieck et al. 2005). The direct interaction of CAST with Bassoon, apparently acting through SNARE complexes, regulates neurotransmitter release (Inoue et al. 2006; Takao-Rikitsu et al. 2004). This raises the possibility that Bassoon *O*-GlcNAcation may play a role in modulating levels of neurotransmitter release through influences on Bassoon protein–protein interactions. In addition to extensive *O*-GlcNAcation, Bassoon is known to be heavily phosphorylated (Collins et al. 2005). Over 30 phosphorylation sites and over 25 *O*-GlcNAc sites have been mapped on mouse Bassoon, and several phosphorylation and *O*-GlcNAc sites map to identical residues. The functions of Bassoon phosphorylation and *O*-GlcNAcation are not known. However, there is almost certainly competition between *O*-GlcNAc and phosphorylation on Bassoon, and it seems likely that such interplay between these post-translational modifications will influence Bassoon scaffolding functions through modulating protein–protein interactions. Although speculative, it is possible that reduced levels of *O*-GlcNAcation in disease states such as AD may facilitate abnormal hyperphosphorylation of Bassoon.

A novel *O*-GlcNAc site was identified on Piccolo within the region APFQYTEGYTTK (residues 3,626–3,637) (supplemental figure 4). Additionally, an *O*-GlcNAc site in human Piccolo homologous to a previously mapped mouse site within the peptide I**TS**NYEVIR (residues 3,974–3,982) (supplemental figure 5) was identified. Piccolo is structurally similar to Bassoon and displays overlapping localization at the cytomatrix of the presynaptic active zone (Fenster et al. 2000). Piccolo, like Bassoon, is heavily phosphorylated and appears to mediate scaffolding functions in neurotransmission (Leal-Ortiz et al. 2008). *O*-GlcNAc may have similar roles in regulating both Bassoon and Piccolo.

Obviously, our sensitivity in identifying *O*-GlcNAc sites in this synaptic sample is quite low. There are most certainly many additional in vivo human *O*-GlcNAc sites to be identified. Lack of sensitivity did not appear to be due to poor enrichment, as the percentage of *O*-GlcNAc modified peptides compared to non-modified in the lectin enriched fraction was similar between mouse and human studies. Loss of sensitivity may be related to the delayed processing of human tissue compared to mouse. Post-mortem delay of human tissue processing has been shown to lead to a rapid reduction in *O*-GlcNAcation levels globally (Liu et al. 2004).

Nevertheless, the overlap of site-specific identifications of *O*-GlcNAc on the synaptic proteins Bassoon, Piccolo, and TPPP/p25 from both mouse and human suggest highly conserved and specific targeting of *O*-GlcNAcation across species, and further support models of potential *O*-GlcNAc regulatory function on these synaptic proteins. Thus, abnormal disease associated levels of *O*-GlcNAcation on such synaptic proteins may contribute to synaptic defects.

Optimization of LTQ ion trap PQD settings for iTRAQ quantitation

Use of the multiplexed differential isotopic quantitation technique iTRAQ in ion trap CID peptide sequencing-based proteomics has been limited by the general absence of low mass range information where iTRAQ reporter ions occur. Recently, PQD fragmentation has been shown to be effective in extending MS/MS information to low mass ranges, making iTRAQ quantitation in ion trap mass spectrometry possible (Griffin et al. 2007; Meany et al. 2007; Bantscheff et al. 2008; Guo et al. 2008). PQD-based ion trap iTRAQ quantitative accuracy is highly dependent on variables in data acquisition including differential collision energies. Previous iTRAQ experiments in LTQ ion trap mass spectrometry used data acquisition in centroid mode (Griffin et al. 2007; Meany et al. 2007), which sums the intensities of about 15 different sampling intervals over an atomic mass unit. The centroid mode is generally preferred, as the scan speed and data processing is faster than "profile" mode, in which averaging is not performed. In profile mode, ion intensity in each of the approximately 15 sampling intervals across an atomic mass unit can be viewed individually, and a peak shape of relative intensity can be visualized in the mass spectrum. We examined the potential use of acquiring iTRAQ PQD MS/MS data in

profile mode in ion trap LTQ mass spectrometry, recognizing that a loss in speed of data acquisition would be a compromise with this strategy. We labeled a tryptic digest of alpha and beta casein with either the 114 or 117 iTRAQ tags and mixed these samples in a ratio of 2.5–1. A total of 500 fmol of this mixture was analyzed by LC–MS/MS utilizing a single CID scan followed sequentially by three identical PQD MS/MS scans of the precursor ion. As reported previously (and data not shown), PQD at all collision energies tested (23–38%) generated much lower intensity peptide fragment ions and performed much more poorly in peptide identification compared to CID (data not shown). We tested the influence of using variable peak widths of iTRAQ reporter ion intensities for use in calculating iTRAQ ratios. A constant optimal collision energy of 33% (see below for optimization of collision energy) was used. Using iTRACKER software (Shadforth et al. 2005), we analyzed the same set of data in three ways; either specifying a mass width around the target iTRAQ reporter ions of ±0.1, 0.25, or 0.5 Da for inclusion of ion intensity in ratio calculations. For peptides identified shown in Table 2, both 0.1 and 0.25 Da settings provided a similarly accurate average ratio quite close to the expected 2.5:1 value. However, the standard deviation of ratio average was much lower when ±0.25 Da was used as the width compared to 0.1 Da (Table 2). The ±0.5 Da width resulted in an average ratio of 3.9 that deviated from the expected 2.5:1 ratio by about 66%, and this included high variability as reflected in the standard deviation of 1.8. Thus, iTRAQ ratios from PQD data acquired in profile mode are sensitive to the peak width used in calculations, and it appears that widening of the peak width past ±0.25 Da with LTQ profile data leads to significant variability in accuracy of iTRAQ quantitation in the LTQ instrument.

The range of PQD collision energy that is optimal for iTRAQ quantitation has been shown to be quite narrow and is likely instrument specific (Griffin et al. 2007; Meany et al. 2007). Thus, we tested a range of collision energies in PQD MS/MS quantitation of iTRAQ labeled alpha and beta casein tryptic digest labeled in a ratio of 7.5:1 with the 114 and 117 tags, respectively, acquiring data in profile mode and calculating ratios using ±0.25 Da width. A total of 500 fmol of the iTRAQ labeled sample was analyzed by LC–MS/MS using a single CID MS/MS scan followed by multiple PQD scans at varying collision energies from 25 to 38%. Indeed, the accuracy of iTRAQ quantitation was quite sensitive to varying collision energies (Table 3). In our case, a setting of 33% collision energy was optimal, generating an average ratio of 7.2:1 for the peptides shown in Table 1, with a standard deviation of 1.1. Collision energies either lower (30%) or higher (36%) led to significantly greater deviation from the expected 7.5:1 ratio (Table 3). Thus, this confirms that choice of collision energy is an important factor that should be intrinsically determined in iTRAQ quantition in ion trap mass spectrometers.

Quantitation of *O*-GlcNAc site-specific modification by iTRAQ

In future studies it will be desirable to determine quantitative site-specific changes in *O*-GlcNAcation in AD and other disease states. However, it is not known how *O*-GlcNAc modification of a peptide may affect iTRAQ labeling or analysis of iTRAQ quantitation. We began to test this by using a synthetically made *O*-GlcNAc modified peptide PSVPV(*S*-*O*-GlcNAc)GSAPGR, which was labeled by four iTRAQ reporter tags (114–117) in a

Table 2 The influence of peak width selection for iTRAQ quantitation of reporter ions acquired in profile mode

Peptide	Ratio 114:117		
	Using peak width 0.1 Da	Using peak width 0.25 Da	Using peak width 0.5 Da
K.VIPYVR. Y	1.5	2.6	3.7
K.TTMPLW	3.2	2.9	3.7
K.EDVPSER. Y	2.1	2.5	6.6
K.EGIHAQQK. E	2.2	2.3	4.1
K.FALPQYLK. T	1.0	2.7	3.0
K.LTEEEKNR. L	3.3	2.0	7.8
R.NAVPITPTLNR. E	2.7	2.8	2.3
R.YLGYLEQLLR. L	3.8	2.9	4.4
K.AMKPWIQPK. T	0.6	3.0	2.1
R.FFVAPFPEVFGK.E	1.8	2.2	1.4
K.HQGLPQEVLNENLLR.F	4.2	2.8	3.7
Average	2.4	2.6	3.9
Standard deviation	1.1	0.3	1.8

Alpha and Beta casein tryptic digests were labeled in a ratio of 2.5:1 with iTRAQ tags 114.1 and 117.1, respectively, and analyzed by LC–MS/MS in profile mode using PQD fragmentation. iTRAKER software was used to calculate experimental 114.1:117.1 ratios using varying widths of 0.1, 0.25, or 0.5 Da surrounding the expected mass of the iTRAQ reporter ion

Table 3 The influence of collision energy in PQD-based iTRAQ quantitation in LTQ ion trap mass spectrometry

Peptide	Ratio 114:117				
	25% CE	30% CE	33% CE	36% CE	38% CE
K.EKVNELSK.D	N/A	3.8100	8.1330	7.2233	N/A
K.EPMIGVNQELAYFYPELFR.Q	N/A	1.3900	8.4222	N/A	N/A
K.HQGLPQEVLNENLLR.F	5.3900	4.3400	5.7100	4.9500	N/A
R.FFVAPFPEVFGK.E	N/A	4.0383	6.9843	3.0633	2.2400
R.YLGYLEQLLR.L	N/A	6.6175	5.9660	7.0267	5.2733
K.ALNEINQFYQK.F	N/A	4.6600	7.6183	6.8067	3.8550
K.ENCLCSTFCCK.E	N/A	7.3825	8.5360	3.7200	6.2667
K.NMAINPSK.E	N/A	5.0800	6.5940	5.6950	3.7600
Average	N/A	4.6648	7.2455	5.4979	4.2790
Standard deviation	N/A	1.8254	1.0996	1.6560	1.5448

Alpha and Beta casein tryptic digests were labeled in a ratio of 7.5:1 with iTRAQ tags 114 and 117, respectively, and analyzed by LC–MS/MS in profile mode using PQD fragmentation at variable collision energies. iTRAKER software was used to calculate experimental 114:117 ratios using a peak width of ±0.25

ratio of 10:5:2.5:1, and analyzed by combined PQD/CID MS/MS and MS/MS/MS on *O*-GlcNAc neutral loss ions as a strategy for simultaneous iTRAQ quantitation and *O*-GlcNAc site mapping. A sample corresponding to 500 fmol of the 114 iTRAQ labeled peptide (50 fmol of the 117 labeled) was analyzed by LC–MS/MS. MS/MS derived from CID fragmentation of the iTRAQ labeled $[M+2H]^{2+}$ precursor at 729.28 gave rise to a characteristic dominant *O*-GlcNAc neutral loss ion at 627.96 (Fig. 4a). This indicates that under these CID conditions, the majority of iTRAQ tag remains covalently attached to the peptide, while the majority of *O*-GlcNAc is dissociated. This is supported by the presence of a fragment ion retaining the iTRAQ label (b2). An ion corresponding to both loss of *O*-GlcNAc and the iTRAQ tag from the intact precursor is not observable in the $[M+2H]^{2+}$ state, but is found in the $[M+2H]^{1+}$ state at 1,110.55 (Fig. 4a), indicating that a fraction of the precursor loses both *O*-GlcNAc and iTRAQ. Indeed, the majority of fragment ions present in MS/MS (although at relative low intensity) correspond to those having lost the iTRAQ tag (Fig. 4a). This indicates that the fraction of peptide having lost the iTRAQ tag more readily fragments along the peptide backbone. The dominant *O*-GlcnAc neutral loss ion in MS/MS still retaining the iTRAQ tag was selected for MS/MS/MS, which gave rise to a spectra dominated by fragment ions which had lost the iTRAQ tag, and which are sufficient to identify this peptide. A single fragment ion (b2) was observed retaining the iTRAQ label. (Fig. 4a). A significant ion corresponding to intact neutral loss precursor showing loss of iTRAQ is observed at 1,110.49 (Fig. 4b) in MS/MS/MS, indicating incomplete fragmentation after loss of the iTRAQ label. Thus, iTRAQ labeled *O*-GlcNAc peptides can be sequenced using CID MS/MS and neutral loss MS/MS/MS strategies. However, it should be noted that a mixture of fragment ions that have both lost and retained the mass of the iTRAQ label may be present in these spectra. The dilution of intensity of these fragment ions between iTRAQ labeled and non-iTRAQ labeled pools may lead to some loss in sensitivity. Our data dependent mass spectrometry method specified a PQD scan of the precursor at collision energy 33% acquired in profile mode subsequent to MS/MS and MS/MS/MS. The low mass range of a PQD spectra corresponding to MS/MS of the *O*-GlcNAc modified peptide is shown (Fig. 4c). Ion intensity within the ±0.25 Da surrounding the expected masses for iTRAQ reporter ions 114–117 was calculated. The observed ratios of 10:4.3:2.4:0.9 correspond well with the expected 10:5:2.5:1 ratio.

Synaptic expression proteomics in AD cortex

We used iTRAQ in LTQ ion trap mass spectrometry to examine potential synaptic expression differences in an AD human cortex versus an age matched non-demented control sample. Hundred micrograms of tryptic digests of synaptic fractions were differentially labeled with iTRAQ tags 114 (control) and 117 (AD), mixed, and subjected to SCX chromatography. Eight SCX fractions were collected and separately analyzed by LC–MS/MS using a method which specified a single CID MS/MS on precursors (for purposes of peptide identification) followed by three sequential PQD scans on the same precursor with data acquired in profile mode and collision energy set at 33%. One hundred and twenty-five proteins were identified for which iTRAQ quantitation was obtained. iTRACKER software (Shadforth et al. 2005) was used to determine iTRAQ 117/114 ratios in PQD scans using a width of ±0.25 Da surrounding

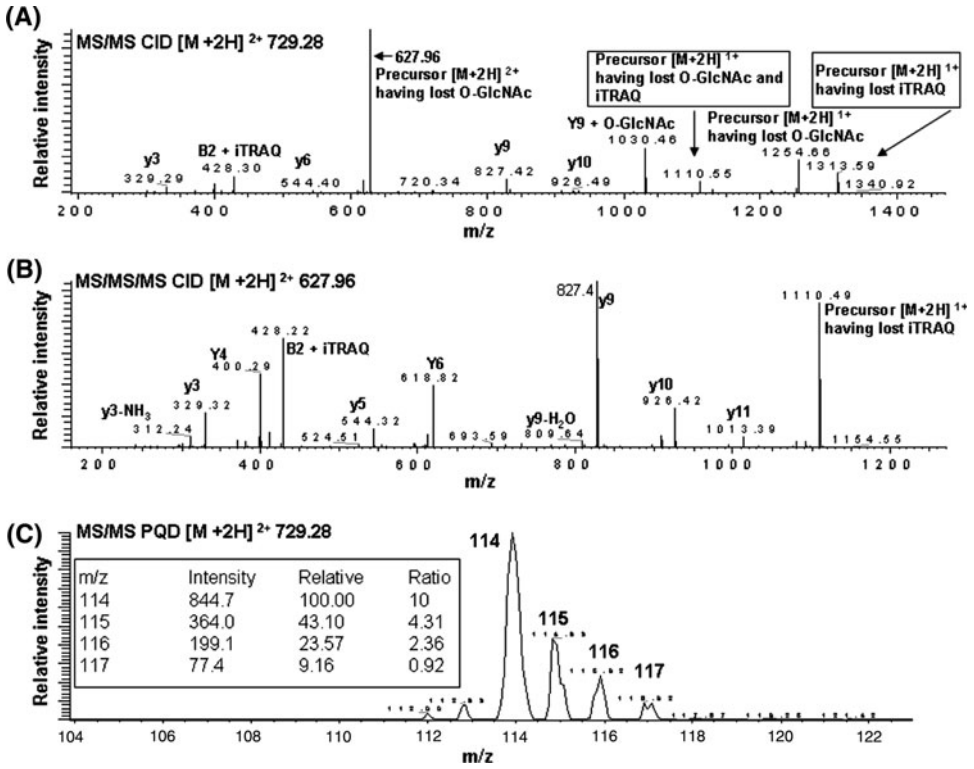

Fig. 4 iTRAQ quantitation of an *O*-GlcNAc modified peptide. The *O*-GlcNAc modified peptide PSVPV(*S*-*O*-GlcNAc)GSAPGR was labeled with iTRAQ differential tags 114, 115, 116, 117 in a ratio of 10:5:2.5:1, respectively, and analyzed by LC–MS/MS using a method specifying CID MS/MS (**a**) which gives rise to a spectra showing the characteristic dominant ion corresponding to the intact precursor having lost the mass of *O*-GlcNAc. This characteristic neutral loss is set to trigger CID MS/MS/MS (**b**) providing greater fragmentation information for peptide sequencing. A subsequent scan was specified in which the original intact precursor is selected for PQD MS/MS (**c**) which allows visualization of iTRAQ reporter ions for relative quantitation (as numerically shown in *inset box*)

the target iTRAQ reporter ion. The raw data of Sequest search algorithm identifications and iTRAQ ratios for each peptide is provided (supplemental table 1).

Twenty-one proteins displayed significantly altered expression in the AD sample (Table 4). HSP70 displayed twofold reduced expression in our AD sample, with an average iTRAQ ratio of AD to control being 0.5 with a standard deviation of 0.02 based on seven unique PQD scans corresponding to HSP70 peptides (Table 4; supplemental table 1). An example of a sequential CID and PQD scans leading to identification and quantitation of a peptide from HSP70 is shown in Fig. 5. Chaperones may in general facilitate presentation of misfolded proteins to the proteasome degradation machinery. Hsp70 and Hsp90 can inhibit amyloid aggregation in neurons (Magrane et al. 2004; Veereshwarayya et al. 2006; Evans et al. 2006) and can recognize AD associated abnormally folded Tau and reduce its levels through facilitating degradation and/or increasing its solubility (Dou et al. 2003; Petrucelli et al. 2004). Reduction of chaperone levels/activity may contribute to accumulation of misfolded/aggregated proteins in AD.

An almost twofold reduction in levels of mitochondrial aldehyde dehydrogenase (ALDH2) was observed (Table 4). Reduced ALDH2 has previously been implicated in neurodegeneration and AD. Oxidative stress and the accumulation of acetaldehyde may play a role in the pathogenesis of AD (Markesbery 1999; Ohta and Ohsawa 2006) and ALDH2 may counter these pathogenic states. ALDH2 deficient cells are sensitive to oxidative insult and ALDH2 can detoxify acetaldehyde accumulation through metabolizing it into acetate (Ohta et al. 2004). A polymorphism that reduces activity of ALDH2 is associated with late onset AD and acts synergistically with a known AD polymorphism in APOE (Kamino et al. 2000). Finally, mice deficient in ALDH2 display neurodegeneration accompanied by memory loss (Ohsawa et al. 2008).

Synapsin II also displayed an almost twofold reduction in the AD sample (Table 4). Synapsins are a family of synaptic vesicle associated proteins that play positive roles in supporting pre-synaptic plasticity through maintance of the availability of synaptic vesicle pools (Fdez and Hilfiker 2006). Mice lacking Synapsins develop learning/memory deficits (Corradi et al. 2008). Thus, potentially reduced Synapsin expression at synapses may contribute to synaptic deficits underlying learning and memory defects in AD.

MAP1B expression was reduced in AD (Table 4). MAP1B may bind microtubles and help stabilize them. Thus, loss of expression and function of MAP1B may contribute to the phenotype of deregulation of microtubule stability observed in AD. Soluble Aβ has been shown to lead to degradation of MAPs including MAP1B (Fifre et al. 2006), consistent with decreased MAP1B levels in our AD sample.

Subunit 7 of the TCP-1/CCT complex which acts to support proper folding of actin and tubulin (Brackley and Grantham 2009) displayed decreased expression in AD,

Table 4 Altered cortical synaptic specific protein expression changes in AD

Protein	Accesion number	117 (AD):114 (control)	
		iTRAQ ratio	Standard deviation
Downregulated in AD			
ATF7IP protein	Q6VMQ6	0.42	0.04
SYN2_HUMAN Synapsin-2 (Synapsin II)	Q92777	0.52	0.03
Serine threonine protein kinase SMG1	Q96Q15	0.46	0.02
Microtubule-associated protein 1B, isoform 1	P46821	0.62	0.02
Heat shock 70 kDa protein 2	P54652	0.50	0.02
Aldehyde dehydrogenase, mitochondrial	P05091	0.55	0.03
Chaperonin containing TCP1 (CCT), subunit 7	Q99832	0.63	0.02
MDHM_HUMAN Malate dehydrogenase	P40926	0.58	0.05
Glyceraldehyde-3-phosphate dehydrogenase	Q2TSD0	0.65	0.08
Internexin neuronal intermediate filament protein	Q16352	0.73	0.06
Beta-tubulin	P07437	0.58	0.10
Upregulated in AD			
Ankyrin repeat and BTB (POZ) domain containing 1	Q969K4	1.82	0.27
Brain creatine kinase	P12277	1.85	0.21
cAMP-dependent protein kinase (PKA) catalytic subunit beta	P22694	2.07	0.48
Glial fibrillary acidic protein	P14136	1.81	0.75
GNAO2_HUMAN Guanine nucleotide-binding protein G(o) subunit	P09471-2	2.43	0.15
Heat shock protein 75 kDa	Q12931	3.27	0.61
N-Acetylglucosamine kinase	Q9UJ70	2.46	0.11
Glutaminase	O94925	2.78	0.13
Septin-4	O43236	1.80	0.07
Ubiquitin carboxyl-terminal hydrolase isozyme L1	P09936	3.64	0.56

Tryptic digests of synaptic fractions were differentially labeled with iTRAQ tags 114 (control) and 117 (AD), and analyzed by LC–MS/MS for peptide/protein identification and iTRAQ ratio determination

raising the idea that such reduced expression may contribute to microtubule disorganization that is observed in AD states.

Glyceraldehyde-3-phosphate dehydrogenase (GAPDH), a glycolytic enzyme, displayed reduced expression in our AD sample. This is consistent with previous reports that suggest GAPDH insoluble aggregation in human AD (Cumming and Schubert 2005) and in AD animal models (Shalova et al. 2007), although the potential relationship to AD pathology is not clear.

Septin 4 overexpression in the AD sample was observed (Table 4). Septins are GTP-binding proteins which can assemble into filaments and function in vesicle trafficking. Septins have been found associated with AD NFTs (Kinoshita et al. 1998) and increased septin 4 specifically linked to neurodegeneration previously (Sitz et al. 2008).

Glial fibrillary acidic protein (GFAP) was overexpressed in our AD sample (Table 4). This is consistent with previous reports of elevated GFAP levels in AD brains (Greber et al. 1999; Ingelsson et al. 2004). While GFAP is a marker of gliosis, GFAP is expressed in hippocampal neurons in the AD state (Hol et al. 2003). GFAP is used a marker of neurodegeration, but its pathological link to AD is not fully understood.

Ubiquitin carboxy-terminal hydrolase L1 (UCH-L1) displayed 3.6-fold increased synaptic expression in our AD sample (Table 4). UCH-L1 is a component of the proteasome degradation pathway and hydrolyzes the C-terminal glycine of ubiquitin, helping to provide a recycling pool of mono-ubiquitin that could be used to label proteins for proteasomal degradation. The proteasomal degradation pathway is known to be down-regulated in Alzheimer's (Keller et al. 2000), which may lead to accumulation of misfolded proteins that would otherwise be degraded. Our observation of increased synaptic levels of UCH-L1 is in contrast to reportedly increased oxidation and reduced expression of UCH-L1 in total AD brains (Choi et al. 2004; Castegna et al. 2002) and in a mouse model of AD (Gong et al. 2006). Abnormal UCH-L1 expression may play a role in AD linked defects in degradation pathways.

The beta subunit of the cAMP-dependent kinase PKA displayed elevated expression in the AD sample (Table 4). PKA is important in hippocampal dependent memory formation (Abel and Nguyen 2008), thus deregulated

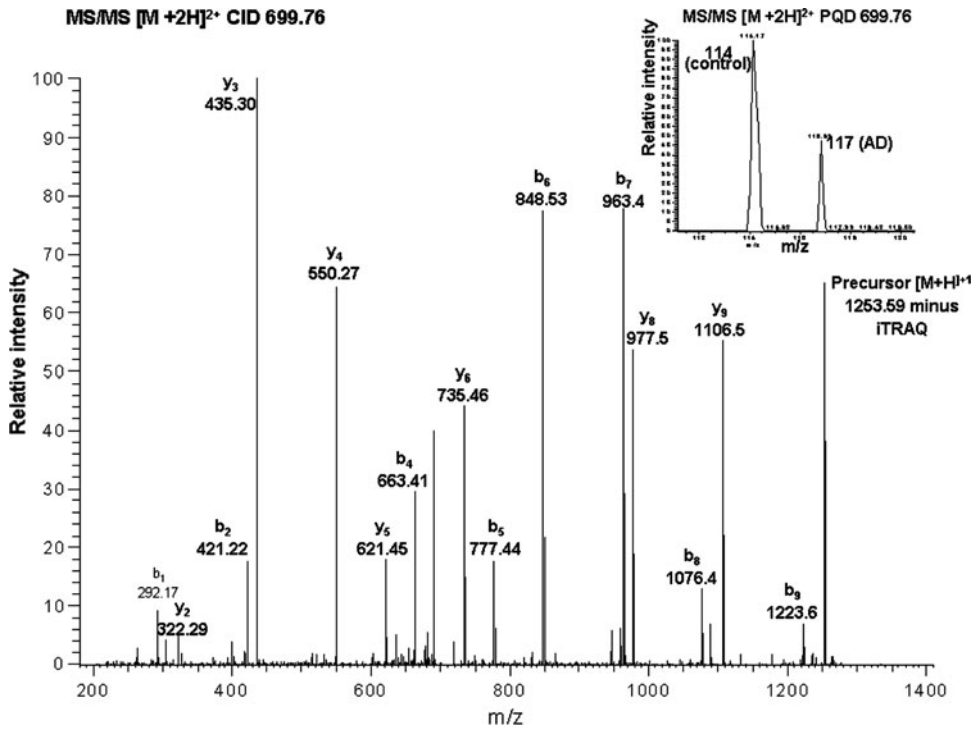

Fig. 5 CID and PQD MS/MS of the peptide FEELNADLFR from HSP70 shows reduced expression in AD cortical synaptic sample. Hundred micrograms of tryptic digests of synaptic fractions were differentially labeled with iTRAQ tags 114 (control) and 117 (AD), mixed, and subjected to strong cation exchange (SCX) chromatography. Eight SCX fractions were collected and separately analyzed by LC–MS/MS using a method which specified a single CID MS/MS on precursors (for purposes of peptide identification) followed by three sequential PQD scans on the same precursor with data acquired in profile mode and collision energy set at 33%. CID MS/MS identifies FEELNADLFR from human HSP70 and inset of a PQD MS/MS example showing *m/z* region of iTRAQ reporter ions revealing decreased expression in the AD sample. Average 117:114 ratio was 0.50 (Table 4)

expression of PKA could possibly contribute to AD related decline in memory formation. Further work will have to be done to confirm the pattern of altered synaptic expression changes observed here.

Discussion

Evidence in rodent systems indicates that *O*-GlcNAc is an abundant modification at neuronal synapses and regulates synaptic plasticity linked to learning/memory (Vosseller et al. 2006; Tallent et al. 2009). Abnormal levels of *O*-GlcNAc in human disease states such as AD may deregulate signaling underlying synaptic plasticity. Thus, we attempted to identify site-specific *O*-GlcNAc modifications in human cortical brain synaptic fractions to begin to understand how synaptic signaling specifically may be influenced by disease associated changes in *O*-GlcNAc levels. The number of sites identified was relatively low, but indicated highly conserved patterns of *O*-GlcNAcation between rodent and human. In particular, a class of proteins which regulates synaptic plasticity through controlling synaptic vesicle distribution (e.g. Bassoon and Piccolo) appears to be heavily *O*-GlcNAc modified in both rodent and human. Bassoon and Piccolo are also extensively phosphorylated. It is quite likely that competition/interplay between *O*-GlcNAc and phosphorylation occur on Bassoon and Piccolo and contributes to their regulation, but this is not yet known. We identified several novel sites of *O*-GlcNAcation on proteins in a human synaptic fraction with known roles in either neurological disease and/or synaptic plasticity. These sites were observed to be proximal to known phosphorylation sites. As in the case of tau, it is tempting to speculate that decreased *O*-GlcNAc in disease states such as AD may in general lead to hyperphosphorylation in cases where a balance of *O*-GlcNAc and phoshorylation is normally maintained at a specific residue through competition. Thus, hyperphosphorylation may be a more general pathologic state in AD due to globally reduced *O*-GlcNAcation.

iTRAQ is a state-of-the-art differential isotopic labeling approach in proteomics. PQD scans enable use of iTRAQ in ion trap mass spectrometry, but accuracy is quite sensitive to variables such as collision energy. A unique feature of iTRAQ is its suitability to the quantitative study of post-translational modifications, as the chemistry will label all peptides in a sample. Other popular differential isotopic quantitative approaches which target subsets of peptides

for expression analysis, such as ICAT (Gygi et al. 1999), will miss many post-translationally modified peptides. We found that iTRAQ quantitiation is compatible with mass spectrometric identification of *O*-GlcNAc modified peptides. Use of iTRAQ should help facilitate more large scale quantitative *O*-GlcNAc comparative proteomic analyses.

Sub-cellular proteomic studies may reveal disease specific changes that would be missed in cruder whole cell/tissue fractions. In addition to neurodegeneration, it is now appreciated that synaptic signaling deficits underlying neuronal plasticity linked to learning and memory occur in AD. We began to examine synaptic specific changes using iTRAQ comparison of protein expression in a cortical synaptic fraction from AD brain versus age matched non-demented control. Several alterations we observed are consistent with previous reports, including elevated levels of Septin-4 and GFAP, and reduced expression of GAPDH and aldehyde dehydrogenase (ALDH2). Several synaptic specific proteins displayed altered expression, including reduced Synapsin II expression in the AD sample. Synapsin levels have not previously been shown to be altered in AD to our knowledge. Possibly, total levels of Synapsin II are unchanged, but mislocalization results in lower synaptic levels in the AD sample.

References

Abel T, Nguyen PV (2008) Regulation of hippocampus-dependent memory by cyclic AMP-dependent protein kinase. Prog Brain Res 169:97–115

Akimoto Y, Comer FI, Cole RN, Kudo A, Kawakami H, Hirano H, Hart GW (2003) Localization of the *O*-GlcNAc transferase and *O*-GlcNAc-modified proteins in rat cerebellar cortex. Brain Res 966:194–205

Arnold CS, Johnson GV, Cole RN, Dong DL, Lee M, Hart GW (1996) The microtubule-associated protein tau is extensively modified with *O*-linked *N*-acetylglucosamine. J Biol Chem 271:28741–28744

Bantscheff M, Boesche M, Eberhard D, Matthieson T, Sweetman G, Kuster B (2008) Robust and sensitive iTRAQ quantification on an LTQ Orbitrap mass spectrometer. Mol Cell Proteomics 7:1702–1713

Brackley KI, Grantham J (2009) Activities of the chaperonin containing TCP-1 (CCT): implications for cell cycle progression and cytoskeletal organisation. Cell Stress Chaperones 14:23–31

Brunet A, Pages G, Pouyssegur J (1994) Growth factor-stimulated MAP kinase induces rapid retrophosphorylation and inhibition of MAP kinase kinase (MEK1). FEBS Lett 346:299–303

Carlin RK, Grab DJ, Cohen RS, Siekevitz P (1980) Isolation and characterization of postsynaptic densities from various brain regions: enrichment of different types of postsynaptic densities. J Cell Biol 86:831–845

Castegna A, Aksenov M, Aksenova M, Thongboonkerd V, Klein JB, Pierce WM, Booze R, Markesbery WR, Butterfield DA (2002) Proteomic identification of oxidatively modified proteins in Alzheimer's disease brain. Part I: creatine kinase BB, glutamine synthase, and ubiquitin carboxy-terminal hydrolase L-1. Free Radic Biol Med 33:562–571

Chalkley RJ, Thalhammer A, Schoepfer R, Burlingame AL (2009) Identification of protein *O*-GlcNAcylation sites using electron transfer dissociation mass spectrometry on native peptides. Proc Natl Acad Sci USA 106:8894–8899

Choi J, Levey AI, Weintraub ST, Rees HD, Gearing M, Chin LS, Li L (2004) Oxidative modifications and down-regulation of ubiquitin carboxyl-terminal hydrolase L1 associated with idiopathic Parkinson's and Alzheimer's diseases. J Biol Chem 279:13256–13264

Cole RN, Hart GW (2001) Cytosolic *O*-glycosylation is abundant in nerve terminals. J Neurochem 79:1080–1089

Collins MO, Yu L, Coba MP, Husi H, Campuzano I, Blackstock WP, Choudhary JS, Grant SG (2005) Proteomic analysis of in vivo phosphorylated synaptic proteins. J Biol Chem 280:5972–5982

Comer FI, Hart GW (2001) Reciprocity between *O*-GlcNAc and *O*-phosphate on the carboxyl terminal domain of RNA polymerase II. Biochemistry 40:7845–7852

Corradi A, Zanardi A, Giacomini C, Onofri F, Valtorta F, Zoli M, Benfenati F (2008) Synapsin-I- and synapsin-II-null mice display an increased age-dependent cognitive impairment. J Cell Sci 121:3042–3051

Cox J, Jackson AP, Bond J, Woods CG (2006) What primary microcephaly can tell us about brain growth. Trends Mol Med 12:358–366

Cumming RC, Schubert D (2005) Amyloid-beta induces disulfide bonding and aggregation of GAPDH in Alzheimer's disease. Faseb J 19:2060–2062

Cunningham C Jr, Glish GL, Burinsky DJ (2006) High amplitude short time excitation: a method to form and detect low mass product ions in a quadrupole ion trap mass spectrometer. J Am Soc Mass Spectrom 17:81–84

Dephoure N, Zhou C, Villen J, Beausoleil SA, Bakalarski CE, Elledge SJ, Gygi SP (2008) A quantitative atlas of mitotic phosphorylation. Proc Natl Acad Sci USA 105:10762–10767

Dou F, Netzer WJ, Tanemura K, Li F, Hartl FU, Takashima A, Gouras GK, Greengard P, Xu H (2003) Chaperones increase association of tau protein with microtubules. Proc Natl Acad Sci USA 100:721–726

Evans CG, Wisen S, Gestwicki JE (2006) Heat shock proteins 70 and 90 inhibit early stages of amyloid beta-(1–42) aggregation in vitro. J Biol Chem 281:33182–33191

Fdez E, Hilfiker S (2006) Vesicle pools and synapsins: new insights into old enigmas. Brain Cell Biol 35:107–115

Fenster SD, Chung WJ, Zhai R, Cases-Langhoff C, Voss B, Garner AM, Kaempf U, Kindler S, Gundelfinger ED, Garner CC (2000) Piccolo, a presynaptic zinc finger protein structurally related to bassoon. Neuron 25:203–214

Fifre A, Sponne I, Koziel V, Kriem B, Yen Potin FT, Bihain BE, Olivier JL, Oster T, Pillot T (2006) Microtubule-associated protein MAP1A, MAP1B, and MAP2 proteolysis during soluble amyloid beta-peptide-induced neuronal apoptosis. Synergistic involvement of calpain and caspase-3. J Biol Chem 281:229–240

Gao Y, Wells L, Comer FI, Parker GJ, Hart GW (2001) Dynamic *O*-glycosylation of nuclear and cytosolic proteins: cloning and characterization of a neutral, cytosolic beta-*N*-acetylglucosaminidase from human brain. J Biol Chem 276:9838–9845

Gong B, Cao Z, Zheng P, Vitolo OV, Liu S, Staniszewski A, Moolman D, Zhang H, Shelanski M, Arancio O (2006) Ubiquitin hydrolase Uch-L1 rescues beta-amyloid-induced decreases in synaptic function and contextual memory. Cell 126:775–788

Gong Y, Lippa CF, Zhu J, Lin Q, Rosso AL (2009) Disruption of glutamate receptors at Shank-postsynaptic platform in Alzheimer's disease. Brain Res 1292:191–198

Greber S, Lubec G, Cairns N, Fountoulakis M (1999) Decreased levels of synaptosomal associated protein 25 in the brain of patients with Down syndrome and Alzheimer's disease. Electrophoresis 20:928–934

Griffin TJ, Xie H, Bandhakavi S, Popko J, Mohan A, Carlis JV, Higgins L (2007) iTRAQ reagent-based quantitative proteomic analysis on a linear ion trap mass spectrometer. J Proteome Res 6:4200–4209

Guo T, Gan CS, Zhang H, Zhu Y, Kon OL, Sze SK (2008) Hybridization of pulsed-Q dissociation and collision-activated dissociation in linear ion trap mass spectrometer for iTRAQ quantitation. J Proteome Res 7:4831–4840

Gygi SP, Rist B, Gerber SA, Turecek F, Gelb MH, Aebersold R (1999) Quantitative analysis of complex protein mixtures using isotope-coded affinity tags. Nat Biotechnol 17:994–999

Gylys KH, Fein JA, Yang F, Wiley DJ, Miller CA, Cole GM (2004) Synaptic changes in Alzheimer's disease: increased amyloid-beta and gliosis in surviving terminals is accompanied by decreased PSD-95 fluorescence. Am J Pathol 165:1809–1817

Hlavanda E, Klement E, Kokai E, Kovacs J, Vincze O, Tokesi N, Orosz F, Medzihradszky KF, Dombradi V, Ovadi J (2007) Phosphorylation blocks the activity of tubulin polymerization-promoting protein (TPPP): identification of sites targeted by different kinases. J Biol Chem 282:29531–29539

Hol EM, Roelofs RF, Moraal E, Sonnemans MA, Sluijs JA, Proper EA, de Graan PN, Fischer DF, van Leeuwen FW (2003) Neuronal expression of GFAP in patients with Alzheimer pathology and identification of novel GFAP splice forms. Mol Psychiatry 8:786–796

Hornbeck PV, Chabra I, Kornhauser JM, Skrzypek E, Zhang B (2004) PhosphoSite: a bioinformatics resource dedicated to physiological protein phosphorylation. Proteomics 4:1551–1561

Husnjak K, Elsasser S, Zhang N, Chen X, Randles L, Shi Y, Hofmann K, Walters KJ, Finley D, Dikic I (2008) Proteasome subunit Rpn13 is a novel ubiquitin receptor. Nature 453:481–488

Ii K, Ito H, Tanaka K, Hirano A (1997) Immunocytochemical co-localization of the proteasome in ubiquitinated structures in neurodegenerative diseases and the elderly. J Neuropathol Exp Neurol 56:125–131

Ingelsson M, Fukumoto H, Newell KL, Growdon JH, Hedley-Whyte ET, Frosch MP, Albert MS, Hyman BT, Irizarry MC (2004) Early Abeta accumulation and progressive synaptic loss, gliosis, and tangle formation in AD brain. Neurology 62:925–931

Inoue E, Deguchi-Tawarada M, Takao-Rikitsu E, Inoue M, Kitajima I, Ohtsuka T, Takai Y (2006) ELKS, a protein structurally related to the active zone protein CAST, is involved in Ca^{2+}-dependent exocytosis from PC12 cells. Genes Cells 11:659–672

Jose M, Nair DK, Altrock WD, Dresbach T, Gundelfinger ED, Zuschratter W (2008) Investigating interactions mediated by the presynaptic protein bassoon in living cells by Foerster's resonance energy transfer and fluorescence lifetime imaging microscopy. Biophys J 94:1483–1496

Kamino K, Nagasaka K, Imagawa M, Yamamoto H, Yoneda H, Ueki A, Kitamura S, Namekata K, Miki T, Ohta S (2000) Deficiency in mitochondrial aldehyde dehydrogenase increases the risk for late-onset Alzheimer's disease in the Japanese population. Biochem Biophys Res Commun 273:192–196

Kanninen K, Goldsteins G, Auriola S, Alafuzoff I, Koistinaho J (2004) Glycosylation changes in Alzheimer's disease as revealed by a proteomic approach. Neurosci Lett 367:235–240

Keller JN, Hanni KB, Markesbery WR (2000) Impaired proteasome function in Alzheimer's disease. J Neurochem 75:436–439

Kinoshita A, Kinoshita M, Akiyama H, Tomimoto H, Akiguchi I, Kumar S, Noda M, Kimura J (1998) Identification of septins in neurofibrillary tangles in Alzheimer's disease. Am J Pathol 153:1551–1560

Klement E, Lipinszki Z, Kupihar Z, Udvardy A, Medzihradszky KF (2010) Enrichment of *O*-GlcNAc modified proteins by the periodate oxidation—hydrazide resin capture approach. J Proteome Res 9(5):2200–2206

Kneass ZT, Marchase RB (2005) Protein *O*-GlcNAc modulates motility-associated signaling intermediates in neutrophils. J Biol Chem 280:14579–14585

Kovacs GG, Gelpi E, Lehotzky A, Hoftberger R, Erdei A, Budka H, Ovadi J (2007) The brain-specific protein TPPP/p25 in pathological protein deposits of neurodegenerative diseases. Acta Neuropathol 113:153–161

Kreppel LK, Blomberg MA, Hart GW (1997) Dynamic glycosylation of nuclear and cytosolic proteins. Cloning and characterization of a unique *O*-GlcNAc transferase with multiple tetratricopeptide repeats. J Biol Chem 272:9308–9315

Lacor PN, Buniel MC, Chang L, Fernandez SJ, Gong Y, Viola KL, Lambert MP, Velasco PT, Bigio EH, Finch CE, Krafft GA, Klein WL (2004) Synaptic targeting by Alzheimer's-related amyloid beta oligomers. J Neurosci 24:10191–10200

LaFerla FM, Oddo S (2005) Alzheimer's disease: Abeta, tau and synaptic dysfunction. Trends Mol Med 11:170–176

Leal-Ortiz S, Waites CL, Terry-Lorenzo R, Zamorano P, Gundelfinger ED, Garner CC (2008) Piccolo modulation of Synapsin1a dynamics regulates synaptic vesicle exocytosis. J Cell Biol 181:831–846

Li X, Lu F, Wang JZ, Gong CX (2006) Concurrent alterations of *O*-GlcNAcylation and phosphorylation of tau in mouse brains during fasting. Eur J Neurosci 23:2078–2086

Lindersson E, Lundvig D, Petersen C, Madsen P, Nyengaard JR, Hojrup P, Moos T, Otzen D, Gai WP, Blumbergs PC, Jensen PH (2005) p25alpha Stimulates alpha-synuclein aggregation and is co-localized with aggregated alpha-synuclein in alpha-synucleinopathies. J Biol Chem 280:5703–5715

Liu F, Iqbal K, Grundke-Iqbal I, Hart GW, Gong CX (2004) *O*-GlcNAcylation regulates phosphorylation of tau: a mechanism involved in Alzheimer's disease. Proc Natl Acad Sci USA 101:10804–10809

Liu F, Shi J, Tanimukai H, Gu J, Grundke-Iqbal I, Iqbal K, Gong CX (2009) Reduced *O*-GlcNAcylation links lower brain glucose metabolism and tau pathology in Alzheimer's disease. Brain 132:1820–1832

Magrane J, Smith RC, Walsh K, Querfurth HW (2004) Heat shock protein 70 participates in the neuroprotective response to intracellularly expressed beta-amyloid in neurons. J Neurosci 24:1700–1706

Markesbery WR (1999) The role of oxidative stress in Alzheimer disease. Arch Neurol 56:1449–1452

Meany DL, Xie H, Thompson LV, Arriaga EA, Griffin TJ (2007) Identification of carbonylated proteins from enriched rat skeletal muscle mitochondria using affinity chromatography-stable isotope labeling and tandem mass spectrometry. Proteomics 7:1150–1163

Oddo S (2008) The ubiquitin-proteasome system in Alzheimer's disease. J Cell Mol Med 12:363–373

Oddo S, Caccamo A, Shepherd JD, Murphy MP, Golde TE, Kayed R, Metherate R, Mattson MP, Akbari Y, LaFerla FM (2003) Triple-transgenic model of Alzheimer's disease with plaques and tangles: intracellular Abeta and synaptic dysfunction. Neuron 39:409–421

Ohsawa I, Nishimaki K, Murakami Y, Suzuki Y, Ishikawa M, Ohta S (2008) Age-dependent neurodegeneration accompanying memory loss in transgenic mice defective in mitochondrial aldehyde dehydrogenase 2 activity. J Neurosci 28:6239–6249

Ohta S, Ohsawa I (2006) Dysfunction of mitochondria and oxidative stress in the pathogenesis of Alzheimer's disease: on defects in the cytochrome c oxidase complex and aldehyde detoxification. J Alzheimers Dis 9:155–166

Ohta S, Ohsawa I, Kamino K, Ando F, Shimokata H (2004) Mitochondrial ALDH2 deficiency as an oxidative stress. Ann N Y Acad Sci 1011:36–44

Ong SE, Mann M (2005) Mass spectrometry-based proteomics turns quantitative. Nat Chem Biol 1:252–262

Ovadi J, Orosz F (2009) An unstructured protein with destructive potential: TPPP/p25 in neurodegeneration. Bioessays 31:676–686

Petrucelli L, Dickson D, Kehoe K, Taylor J, Snyder H, Grover A, De Lucia M, McGowan E, Lewis J, Prihar G, Kim J, Dillmann WH, Browne SE, Hall A, Voellmy R, Tsuboi Y, Dawson TM, Wolozin B, Hardy J, Hutton M (2004) CHIP and Hsp70 regulate tau ubiquitination, degradation and aggregation. Hum Mol Genet 13:703–714

Ross PL, Huang YN, Marchese JN, Williamson B, Parker K, Hattan S, Khainovski N, Pillai S, Dey S, Daniels S, Purkayastha S, Juhasz P, Martin S, Bartlet-Jones M, He F, Jacobson A, Pappin DJ (2004) Multiplexed protein quantitation in *Saccharomyces cerevisiae* using amine-reactive isobaric tagging reagents. Mol Cell Proteomics 3:1154–1169

Rowan MJ, Klyubin I, Cullen WK, Anwyl R (2003) Synaptic plasticity in animal models of early Alzheimer's disease. Philos Trans R Soc Lond B Biol Sci 358:821–828

Schubert D (2005) Glucose metabolism and Alzheimer's disease. Ageing Res Rev 4:240–257

Schwartz JC, Syka JP, Quarmby ST (2005) In: Presented at the 53rd ASMS conference on mass spectrometry, San Antonio, TX, June 5–9

Selkoe DJ (2002) Alzheimer's disease is a synaptic failure. Science 298:789–791

Shadforth IP, Dunkley TP, Lilley KS, Bessant C (2005) i-Tracker: for quantitative proteomics using iTRAQ. BMC Genomics 6:145

Shalova IN, Cechalova K, Rehakova Z, Dimitrova P, Ognibene E, Caprioli A, Schmalhausen EV, Muronetz VI, Saso L (2007) Decrease of dehydrogenase activity of cerebral glyceraldehyde-3-phosphate dehydrogenase in different animal models of Alzheimer's disease. Biochim Biophys Acta 1770:826–832

Sharma P, Veeranna, Sharma M, Amin ND, Sihag RK, Grant P, Ahn N, Kulkarni AB, Pant HC (2002) Phosphorylation of MEK1 by cdk5/p35 down-regulates the mitogen-activated protein kinase pathway. J Biol Chem 277:528–534

Sitz JH, Baumgartel K, Hammerle B, Papadopoulos C, Hekerman P, Tejedor FJ, Becker W, Lutz B (2008) The Down syndrome candidate dual-specificity tyrosine phosphorylation-regulated kinase 1A phosphorylates the neurodegeneration-related septin 4. Neuroscience 157:596–605

Sumegi M, Hunyadi-Gulyas E, Medzihradszky KF, Udvardy A (2003) 26S proteasome subunits are *O*-linked *N*-acetylglucosamine-modified in *Drosophila melanogaster*. Biochem Biophys Res Commun 312:1284–1289

Sweatt JD (2004) Mitogen-activated protein kinases in synaptic plasticity and memory. Curr Opin Neurobiol 14:311–317

Takao-Rikitsu E, Mochida S, Inoue E, Deguchi-Tawarada M, Inoue M, Ohtsuka T, Takai Y (2004) Physical and functional interaction of the active zone proteins, CAST, RIM1, and Bassoon, in neurotransmitter release. J Cell Biol 164:301–311

Tallent MK, Varghis N, Skorobogatko Y, Hernandez-Cuebas L, Whelan K, Vocadlo DJ, Vosseller K (2009) In vivo modulation of *O*-GlcNAc levels regulates hippocampal synaptic plasticity through interplay with phosphorylation. J Biol Chem 284:174–181

tom Dieck S, Altrock WD, Kessels MM, Qualmann B, Regus H, Brauner D, Fejtova A, Bracko O, Gundelfinger ED, Brandstatter JH (2005) Molecular dissection of the photoreceptor ribbon synapse: physical interaction of Bassoon and RIBEYE is essential for the assembly of the ribbon complex. J Cell Biol 168:825–836

Veereshwarayya V, Kumar P, Rosen KM, Mestril R, Querfurth HW (2006) Differential effects of mitochondrial heat shock protein 60 and related molecular chaperones to prevent intracellular beta-amyloid-induced inhibition of complex IV and limit apoptosis. J Biol Chem 281:29468–29478

Vosseller K, Trinidad JC, Chalkley RJ, Specht CG, Thalhammer A, Lynn AJ, Snedecor JH, Guan S, Medzihradszky KF, Maltby DA, Schoepfer R, Burlingame AL (2006a) *O*-GlcNAc proteomics of postsynaptic density preparations using lectin weak affinity chromatography (LWAC) and mass spectrometry. Mol Cell Proteomics 5(5):923–934

Vosseller K, Trinidad JC, Chalkley RJ, Specht CG, Thalhammer A, Lynn AJ, Snedecor JO, Guan S, Medzihradszky KF, Maltby DA, Schoepfer R, Burlingame AL (2006b) *O*-linked *N*-acetylglucosamine proteomics of postsynaptic density preparations using lectin weak affinity chromatography and mass spectrometry. Mol Cell Proteomics 5:923–934

Wells L, Vosseller K, Hart GW (2003) A role for *N*-acetylglucosamine as a nutrient sensor and mediator of insulin resistance. Cell Mol Life Sci 60:222–228

Xu B, Wilsbacher JL, Collisson T, Cobb MH (1999) The N-terminal ERK-binding site of MEK1 is required for efficient feedback phosphorylation by ERK2 in vitro and ERK activation in vivo. J Biol Chem 274:34029–34035

Yao PJ, Coleman PD (1998) Reduced *O*-glycosylated clathrin assembly protein AP180: implication for synaptic vesicle recycling dysfunction in Alzheimer's disease. Neurosci Lett 252:33–36

Yao T, Song L, Xu W, DeMartino GN, Florens L, Swanson SK, Washburn MP, Conaway RC, Conaway JW, Cohen RE (2006) Proteasome recruitment and activation of the Uch37 deubiquitinating enzyme by Adrm1. Nat Cell Biol 8:994–1002

Yates JR 3rd, Eng JK, McCormack AL, Schieltz D (1995) Method to correlate tandem mass spectra of modified peptides to amino acid sequences in the protein database. Anal Chem 67:1426–1436

Yuzwa SA, Macauley MS, Heinonen JE, Shan X, Dennis RJ, He Y, Whitworth GE, Stubbs KA, McEachern EJ, Davies GJ, Vocadlo DJ (2008) A potent mechanism-inspired *O*-GlcNAcase inhibitor that blocks phosphorylation of tau in vivo. Nat Chem Biol 4:483–490

Zhang F, Su K, Yang X, Bowe DB, Paterson AJ, Kudlow JE (2003) *O*-GlcNAc modification is an endogenous inhibitor of the proteasome. Cell 115:715–725